127

PHYSICAL REVIEW LETTERS

Published week ending 24 SEPTEMBER 2021

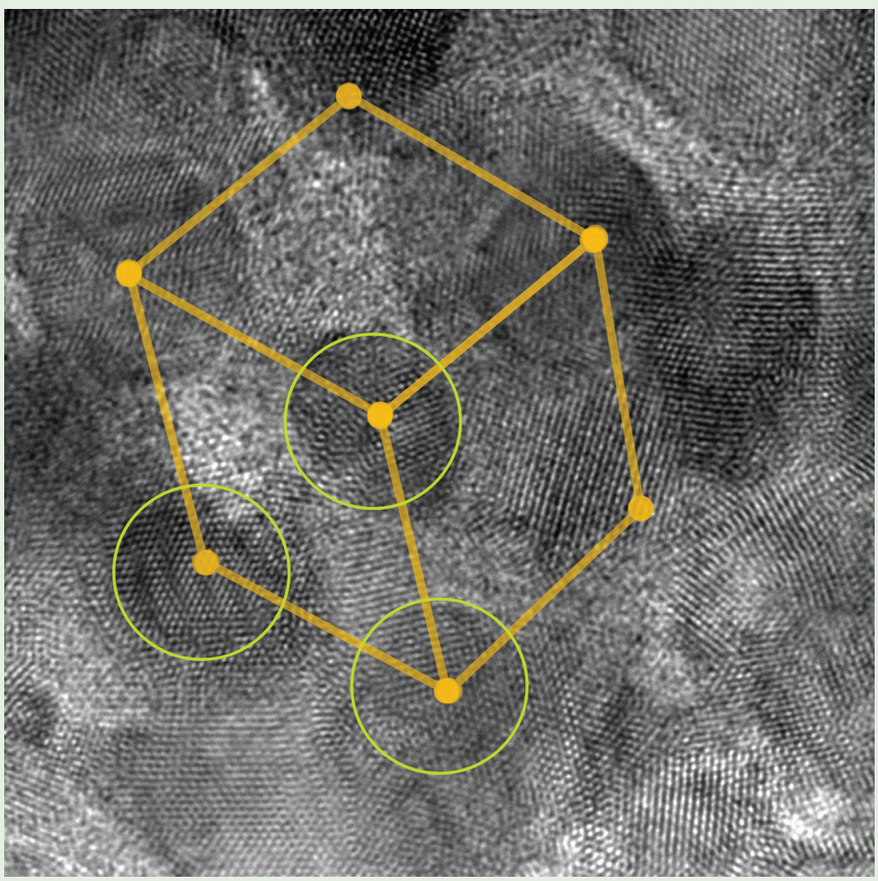

PRL 127 (13), 130401–139902, 24 September 2021 (296 total pages)

13

Published by
American Physical Society

APS physics

Volume 127, Number 13

Formation of Stable Schwarz Crystals in Polycrystalline Copper at the Grain Size Limit

Zhaohui Jin,* Xiuyan Li,† and K. Lu‡
Shenyang National Laboratory for Materials Science, Institute of Metal Research, Chinese Academy of Sciences, Shenyang 110016, China

(Received 11 July 2021; accepted 10 August 2021; published 20 September 2021)

A prototype Schwarz crystal (SC) structure of dividing–space minimal grain boundaries (GBs) constrained by coherent twin boundaries (CTBs) was recently discovered in extremely fine-grained polycrystalline Cu. In this Letter, constraining effects of 3*D* CTB network on the formation and thermostability of SC are addressed via atomistic simulations. GB migration and evolution of CTB network trigger formation of SC *diamond*. CTB constraints are critical to generate GBs of zero mean curvature underlying vanishing capillary pressure, and to counterbalance the elastic driving forces of lattice. GB motion can be suppressed at temperatures close to the melting point with GB aperture down to 3 nm.

DOI: 10.1103/PhysRevLett.127.136101

In polycrystalline copper consisting of grains of a few nanometers in size, a metastable structure was discovered in which grain boundaries (GBs) constrained by quadrupolar network of coherent twin boundaries (CTB) resemble essentially the triply periodic minimal surface (*TPMS*) of Schwarz primitive diamond (*D*), as illustrated in Fig. 1. Such polycrystalline structures of metals are found to exhibit superior thermal and mechanical stabilities than any other forms of metastable solid states known so far, for example, the metallic glasses. The extremely fine-grained structures with GB or interfacial morphologies featured by any topological manifold of minimal surface, called *Schwarz crystal* (SC), may represent a novel type of intrinsic metastable state in polycrystalline metals at an ultimate grain size limit [1].

The combination of experiments, atomistic modeling and simulations evidenced that SC of pure Cu remains stable, either in grain morphology or in grain size, at temperatures close to the equilibrium melting point of the bulk lattice (T_E, 1358 K). It is remarkably hard at room temperatures, with an ideal strength (more than 2 GPa) close to the theoretical limit. The structure does not break down in a sudden way prior to significant plastic deformations under tensile loading in the entire temperature range. Similar structures and behaviors are also observed in other face-centered-cubic (fcc) metals such as pure Al and Al-Mg alloys [20,21]. Exampled with Cu, the present study aims to address the transformation of Schwarz crystals from nanograined polycrystals with molecular dynamics (MD) simulations. Structural characteristics and thermal stabilities of Schwarz crystals are analyzed and compared with experimental observations.

As a first concrete and successful mathematical solution of Plateau's problem, perhaps the Schwarz primitive *D* surface, together with primitive *P* surface, are of most frequently mentioned *TPMS*s in mathematics and physics [22,23]. The minimal *P* and *D* surface are also closely related to the gyroid in that they are contained in the same associate (Bonnet $\mathbf{R}^3$) family [2,24–26]. In Fig. 1(a), the form of unit *D* surface in a cubic cell can be viewed as a skew quadrilateral with two pairs of sides of equal lengths, each embedded in one tetrahedron (such as *ADjq* or *Bijh* and so on), expended in certain series as an [111] orientated enclosure. The smooth surface contains infinite numbers of straight lines and is of zero mean curvature everywhere. As the surface triply fills up the space, the cubic box fulfills the 3D periodic boundary conditions as a supercell.

Whether *TPMS* morphologies occur in condensed matter is always intriguing [27–30]. Consider the supercell in Fig. 1(a) as part of a bulk fcc lattice (e.g., Cu) in ⟨100⟩ cubic orientations, it is by no means apparent that embedding the *D* surface would result in a structural unit both space filling and stable, as in doing so, GBs other than the *D* surface could be generated due to crystallographic division of space. Although we know now both general GB and special CTB in the Schwarz *D* crystal mutually constitute one symmetric solution of a unit cell representing a new form of the metastable state in fcc metals such as Cu [Fig. 1(b)], we did not tackle the problem in this way in the beginning. An alternative approach, the well-known Kelvin conjecture [31], has been initially implemented in our modeling and simulations, inspired by concept such as how possibly a CTB network may form in space, based on that truncated octahedron-shaped grains and numerous CTBs are frequently observed in extremely fine-grained metals like Cu revealing meanwhile an enhanced thermostability [1,32,33].

As revealed in Fig. 1(c) and Fig. 2, starting from Kelvin packing of sixteen truncated octahedral grains in such a way that grains O1 and O2 of ⟨100⟩ cubic lattice orientations are surrounded by those of strictly specified ⟨112⟩ orientations, a space-filling 3D CTB (Σ3) network can be constructed, merged with other GBs of Σ9 families formed by ⟨$\bar{1}$22⟩, ⟨$\bar{1}$84⟩, and ⟨44$\bar{7}$⟩ orientated grains [Fig. 2(a) and

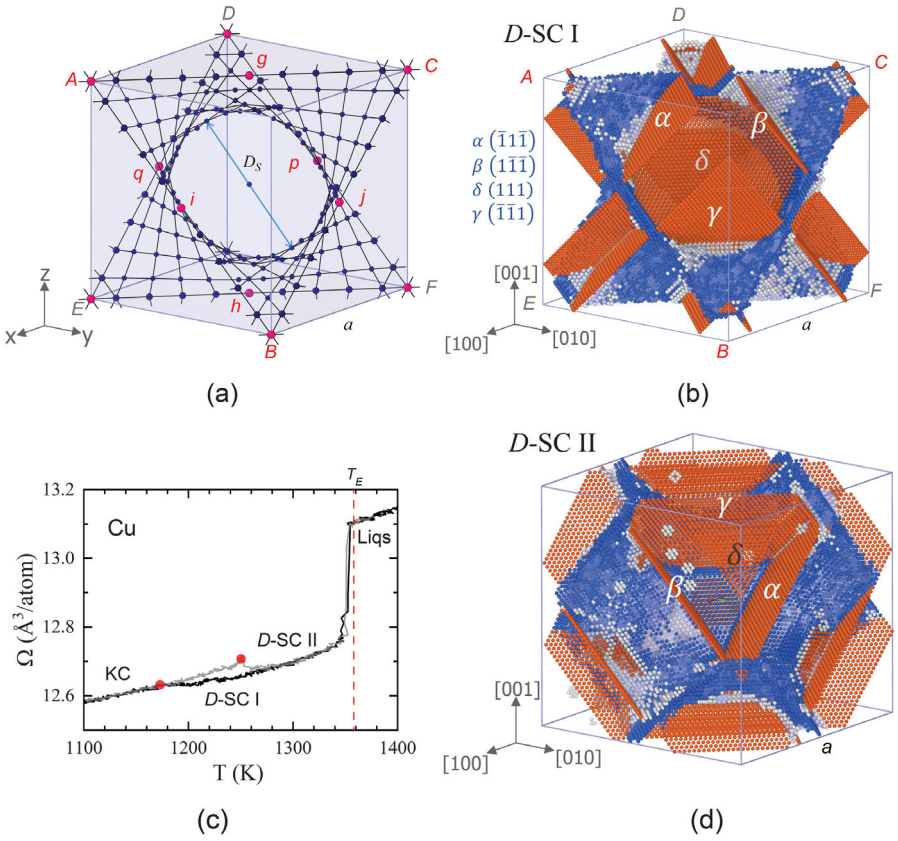

FIG. 1. (a) Schwarz D-TPMS based on exact mathematical solution [2]. The unit cell contains 6 primitive patches around [111] axis, each enclosed by a tetrahedron such as "$ADgq$" or "$Agqi$". The aperture of a $D-SC$ is defined as $D_S=\sqrt{2}/2a$. (b) Schwarz crystal (SC) of type–I D-surface morphology (D–SC I, $a\sim 13$ nm) observed in MD simulations of Cu. GB atoms colored in gray are recolored in blue if locating within a surface layer of 1 nm thick according to Eq. (1). Atoms at CTB sites are colored in orange. Atoms in fcc lattice sites are filtered out. (c) The two MD-obtained thermal profiles (atomic volume vs temperature) indicate that the transformations from twin-limited Kelvin crystal (KC, denoted as 'KC0' in the Supplemental Material [3]) occur at 1172 K to D–SC I or at 1250 K to D–SC II well below the T_E (1358 K) of Cu. (d) The same KC may transform into a D–SC II ($a\sim 13$ nm) with a different partition of D surface [Eq. (1) with a spatial translation of $\pi/2$], depending on intergranular interactions and thermal activations.

the Supplemental Material [3]]. Such a unique Kelvin crystal (KC) may transform into a SC via thermal activations or aided by mechanical stimuli (Ref. [1] and Supplemental Material [3]). In our present case, the structural transition from KC to SC occurs upon heating [Fig. 1(c)] during which the same KC may transform either into an SC shown in Fig. 1(b) (D–SC I) or into that shown in Fig. 1(d) (D–SC II).

GB atoms belong to a $TPMS$ can be easily identified since such surfaces can be represented using trigonometric functions [34]. Specifically, the level functions can be defined as

$$S_D(\tilde{x},\tilde{y},\tilde{z})=\sin\tilde{x}\sin\tilde{y}\sin\tilde{z}+\sin\tilde{x}\sin\tilde{y}\cos\tilde{z}+\cos\tilde{x}\sin\tilde{y}\cos\tilde{z}+\cos\tilde{x}\cos\tilde{y}\sin\tilde{z}=0 \quad (1)$$

for the Schwarz D surface and

$$S_P(\tilde{x},\tilde{y},\tilde{z})=\cos 2\tilde{x}+\cos 2\tilde{y}+\cos 2\tilde{z}=0 \quad (2)$$

for the Schwarz P surface, where $\tilde{x}$, $\tilde{y}$, $\tilde{z}$ are reduced Cartesian coordinates of atoms, defined as $\tilde{x}=x\cdot m\pi/l_x$, $\tilde{y}=y\cdot n\pi/l_y$ and $\tilde{z}=z\cdot p\pi/l_y$ for an orthogonal box containing $m\times n\times p$ fundamental cell units of SC with respect to X (100), Y (010), and Z (001) lattice directions. In both Fig. 1(b) and Fig. 1(d), more than 80% of GB atoms (colored in ink blue) are found within a surface layer of about 1 nm thickness according to Eq. (1), i.e., $|S_D(\tilde{x},\tilde{y},\tilde{z})|\le 0.15$ for D–SC I or $|S_D(\tilde{x}-\pi/2,\tilde{y}-\pi/2,\tilde{z}-\pi/2)|\le 0.15$ for D–SC II, where m, n, $p=1$ and l_x, l_y, $l_z=a\approx 13$ nm.

Figure 2(a), (a)–(f) illustrate the transformation from the KC into the Schwarz crystal DSC I. The transition occurs at ~1172 K [Fig. 1(c)] at an expense of all grains except O1 and O2. Those grains finally disappear when decomposed GBs are constricted into single GBs ($D-TPMS$) due to simultaneous expansion of preexisting CTBs associated with O1 and O2 along the CTB network channels (as marked, "*longitudinal*"). Figure 2(b), (i)–(p) illustrate the transformation from KC to D–SC II at a higher onset temperature (~1250 K) due to simultaneous expansion of the CTB network but in different orientations (as marked, "*transverse*"). Rising up the temperature further, both SCs

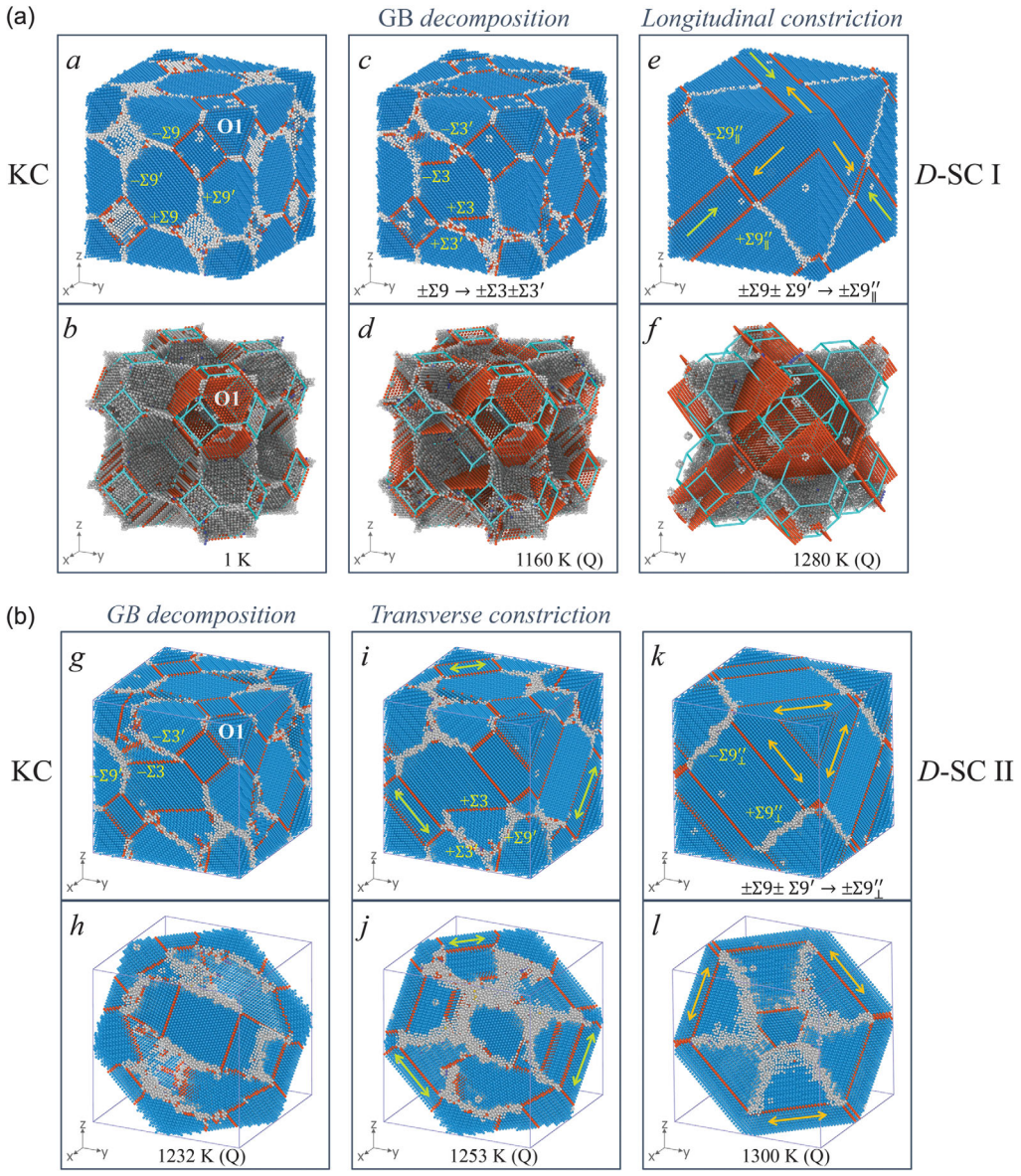

FIG. 2. Transformations from KC to *D*–SC corresponding to Fig. 1(c). (A) KC to *D*–SC I via '*longitudinal*' constriction of GBs. (a)–(f) Snapshots of MD configurations at different temperatures. Thermal noises are eliminated from MD configurations via energy minimizations (indicated by Q as "quenched" state). Frames of initial Kelvin cells are drawn in (b), (d) and (f) to reveal the structural evolution, where atoms in fcc lattice sites colored in blue in (a), (c) and (e) are removed. (B) KC to *D*–SC II via '*transverse*' constriction of GBs. (g)–(l) Quenched states of MD configurations at different temperatures. To reveal GB activities, the [111] foils (~1.5 nm thick) are shown in (h), (j) and (i). For KC, both O1 and O2 locate in the [111] orientation but sit apart from each other at a distance of $a\sqrt{3}/2$ as explicitly shown in Fig. S1 of the Supplemental Material [3].

transform into the liquid states initiated by heterogenous GB melting, underlying that the migration of GBs in SC can been completely suppressed at temperatures close to the melting point [Fig. 1(c)].

At low homologous temperatures ($T < T_E/3$), a Σ9 GB formed by $\langle\bar{1}22\rangle$ oriented grains may readily dissociate into a Σ3 CTB and a Σ3′ GB (*none*–CTB) according to $\pm\Sigma9 \rightarrow \pm\Sigma3 \pm \Sigma3'$ [35–37], where $\pm$ distinguishes opposite directions of GB plane normal. The decomposition occurs preferentially at corners (quadrupolar points, QPs) and edges (triple lines, TLs) of the initial GB network [Fig. 2(a)], such that the KC can be energetically relaxed. Meanwhile, since the decomposed GBs are intrinsically mobile, it also leads to enhanced geometry complications, resulting in significant precursor effect that may influence the way how the CTB network expands (*longitudinal* or *transverse*) to trigger transformation from KC to SC at high temperatures. Interestingly, the constriction into Schwarz *D*–GB does not occur due to annihilation of dissociated GBs of opposite signs, but rather via the combination of Σ9 GBs, i.e., $\pm\Sigma9 \pm \Sigma9' \rightarrow \pm\Sigma9''$, by which reversed GB reactions, i.e., $\pm\Sigma3 \pm \Sigma3' \rightarrow \pm\Sigma9$, are involved.

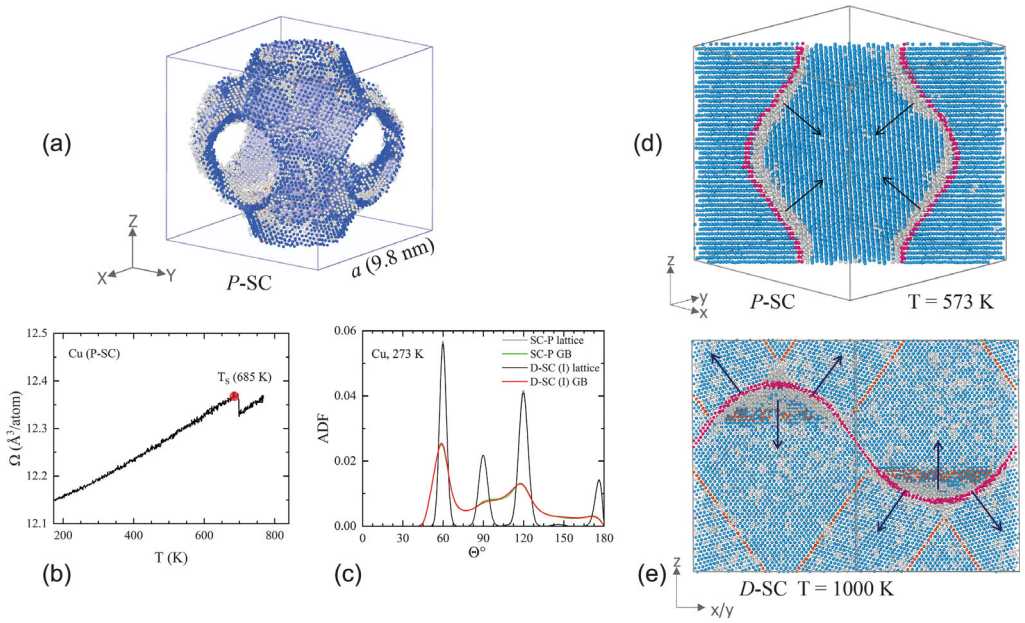

FIG. 3. (a) *TPMS* GBs of a twin-free primitive Schwarz crystal (*P*–SC, constructed using two Kelvin cells of equal size) in a fully relaxed MD configuration at 0 K. More than 80% of GB atoms (colored in blue) are within the surface layer of ∼1.5 nm thick according to Eq. (2). (b) MD-obtained thermal profile of atomic volume as a function of temperature. Upon heating, the *P*-SC remains stable up to 685 K ($0.5T_E$) at which opposite GBs shrink toward each other and annihilate abruptly. (c) ADFs calculated for GB atoms and lattice atoms in *P*-SC and *D*-SC. Similar GB structures and certain degree of disorders typical for general GBs are well expected for both SCs. (d) The [110] cross section view of the *P*-SC at 573 K. Atoms in red mark the trace of *P* surface according to Eq. (2). (e) The [110] cross section view of a *D*-SC at 1000 K. Atoms in red mark the trace of the *D* surface according to Eq. (1). CTB constraining effects are schematically represented by arrows underlying counterbalanced and hence vanishing GB tension forces for GB motion.

Our MD observations revealed that the transformation from KC to SC is strongly constrained by the 3*D*-CTB network, through which nodes (QPs) and edges (TLs) of the GB network in a KC can be completely eliminated. Individual grains disappear via enhanced activities such as GB reactions. The original GB network is replaced by a new one, through which the total GB area is minimized effectively and the unique morphology of the Schwarz *D*-minimal surface is adopted.

Since GBs in a Schwarz crystal are of vanishing curvature, the capillary pressure (P) on the GB is minimal ($P \to 0$) according to the Young-Laplace law

$$P = 2\gamma_{GB}/R, \tag{3}$$

where γ_{GB} is the GB energy and R is the mean GB radius of curvature. However, deviation from the minimal curvature condition is expected because significant thermal fluctuations is inevitable at high temperatures.

An additional pressure (S) may also arise when neighboring lattices of the GB are under an appreciable stress (τ)

$$S = \frac{\tau^2}{2}\left(\frac{1}{E_A} - \frac{1}{E_B}\right), \tag{4}$$

where E_A and E_B are Young's moduli of neighboring grains A and B, respectively [38]. Since a crystalline lattice is intrinsically anharmonic and anisotropic, $E_A \neq E_B$, which means thermally a persisting driving force tends to be imposed for GB motion. When deviate away from the *TPMS* morphology, GB migration constitutes the major mode of motion although it may be coupled with other activities such as GB sliding [39]. Suppose that the critical pressure for GB migration is P_c, the temperature (T_S) at which a SC is rendered thermally unstable can then be measured by

$$p(T_S) = P(T_S) + S(T_S) = P_c. \tag{5}$$

The T_S of CTB-free *TPMS* GBs can be assessed using a SC in Schwarz *P* form (*P*-SC) by Kelvin packing of two truncated octahedral grains. A *P*-SC with $\pm\Sigma 9''$–type GBs similar to those in *D*-SC has been shown in Fig. 3(a). The GB energy is calculated to be $\gamma_{\mathrm{GB}} \sim 1$ eV/m^2 (0 K) given that the GB area (A_{GB}) is known exactly, which is $\sim 2.35a^2$ for *P*-SC and $\sim 2.42a^2$ for *D*-SC [2,26]. Such a *P*-SC is thermally stable up to 680 K at which GBs collapse promptly [Fig. 3(b)]. That is, either for *P*-SC or for *D*-SC, GBs of minimal surface are intrinsically mobile defects which would readily migrate at $T_S \sim 0.5T_E$. Structure analyses in terms of the 1st nearest-neighbor angular distribution function (ADF) indicate that significant amount of GB atoms is disordered [Fig. 3(c)], underlying that the GB migration is assisted by thermally activated GB diffusivities. Figure 3(d) shows that substantial nonvanishing GB curvature can be developed at temperatures below T_S.

CTB constraints are essential to account for the unusual thermostability of $T_S \sim 0.98T_E$ achieved by D-SC I/II. Since twinned lattices show up successively on both sides of the GB, the driving forces imposed on different portions of GB are of the same magnitude but in opposite directions [Eq. (4) and Fig. 3(e)], by which a minimal pressure condition holds up to the melting point of GB, irrespective of thermal fluctuations and P_c, i.e., at $T \leq T_m^{\mathrm{GB}}$

$$\langle S(T) \rangle \to 0, \tag{6}$$

or

$$p(T) = P(T) + \langle S(T) \rangle \to 0, \tag{7}$$

where $\langle \ldots \rangle$ denotes the mean driving force under CTB constrains. As an alternative evidence of Eq. (6), both D-SC I and II are found ideally isotropic according to our calculated elastic moduli (see Supplemental Material [3]), in accordance with the zero–pressure condition ($E_A = E_B$) of Eq. (4). In short, the structures of Schwarz D-GBs bound together with CTBs represent the case where the mean driving force for GB migration is also minimal even at temperatures close to T_E, a condition difficult to attain otherwise.

D-SC I and II of smaller sizes (a) also form (see Supplemental Material [3]). The KC–to–SC transformation temperature drops down when a KC is constructed with smaller Kelvin cells. The limiting thermostability measured by T_S/T_E as a function of the aperture size of D-SC (D_S) has been illustrated in Fig. 4(a). Among them, S0 and S1 are found most stable and GB migration can be completely suppressed at temperatures close to the melting point above a size limit of $D_S = 3$ nm. Smaller D-SCs, on the other hand, can be destabilized as a consequence of CTB and/or GB annihilation. The onset temperature of destabilization drops down significantly from $0.94T_E$ (S2) to $0.4T_E$ (S4). For S4, the tiny cell contains merely 3016 atoms and nearly one third of them can be identified as GB atoms, enhanced GB interactions must account for the instability. Yet, comparing to conventional polycrystals, a thermal stability of $0.4T_E$ is still promising at such a grain size regime.

Identifying the D-SC morphology at atomic scales remains challenging experimentally because the topological structure contains high-density GBs and CTBs. However, the structural symmetries of D-SC I as revealed in Fig. 1(a) and Fig. 4(b) provide following hints. (i) The $\langle 111 \rangle$ channels of D-SC should be most transparent to electron beams because only one set of CTBs shows up in each aperture normal. (ii) Electron beams are less transparent along $\langle 0\bar{1}1 \rangle$ orientations as all sets of CTBs $(\alpha, \beta, \gamma, \delta)$ show up and incline to each other. (iii) Along all other orientations, electrons tend to be scattered away due to highly disordered GB atoms and overlapped GBs. As such, symbolic honeycombed grains of circular shape or manifolded bright and dark strips are observable experimentally, as shown in Fig. 4(c) or Fig. 1 in Ref. [1].

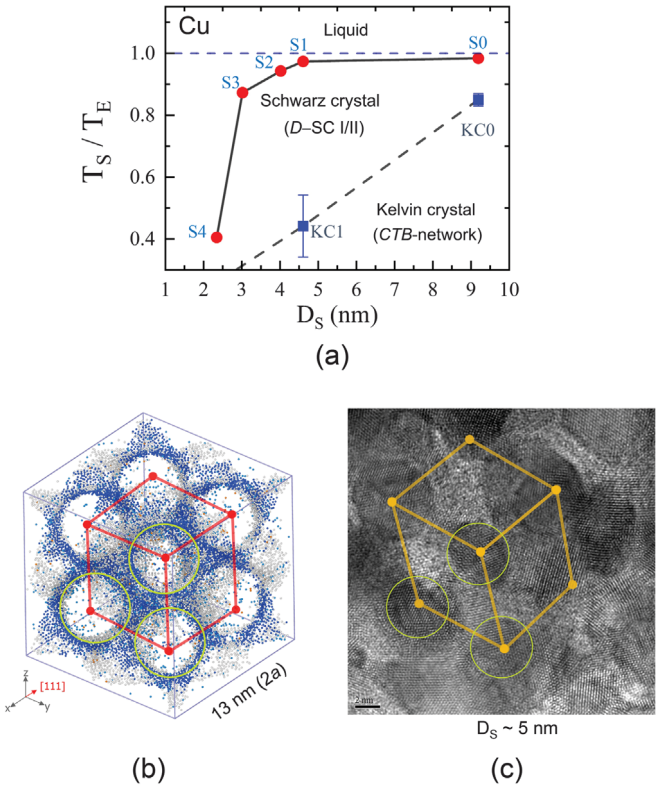

FIG. 4. (a) Size dependence of D-SC thermostability, T_S/T_E vs D_S. The temperature range of KC–to–SC transformation is marked by the dashed line and error bars. Here, S0, S1, S2, S3, and S4 stand for D-SC structures obtained upon transformations from KCs of various supercell sizes, i.e., $a \cong$ 13 nm (KC0), 6.5 nm (KC1), 5.7 nm (KC2), 4.3 nm (KC3), and 3.3 nm (KC4), see additional details in the Supplemental Material [3]. (b) MD snapshot of a D–SC I at 473 K, containing 8 ($2 \times 2 \times 2$) unit cells of $a \sim 6.5$ nm and $D_S \sim 4.6$ nm. (c) A HRTEM image of an as-prepared sample of Schwarz crystal Cu, from which a D–SC morphology can be deduced ($D_S \sim 5$ nm). Also similar to MD observations, the structure is thermally stable up to nearly 1350 K according to experimental measurements [1].

Understanding the nature of GBs and interfaces is vital to predict material properties [40–43]. With this study, we demonstrated that limiting grain size of a few nanometers is approachable in conventional metals if an interface network is prone to a unique form underlying remarkable thermal stability. Our simulations show that in Schwarz D-crystals, *TPMS* GBs remain to be lattice defects highly energetic and intrinsically mobile. However, distinct from those as conjectured by Kelvin crystals, they are stable topological defects of vanishing mean curvature. GBs of much lower energies and intrinsically less mobile, such as CTBs in fcc metals, remain to be planar defects and may act as strong constraints against GB motion. Schwarz crystals, including those of lattice structures of other types, point the way for future advances of structurally stable materials.

This work is funded by the Ministry of Science and Technology of China (Grants No. 2017YFA0204401 and

No. 2017YFA0700700) and the Chinese Academy of Sciences. We thank Dr. X. Zhou for assistance in experiments. Part of the MD calculations were carried out using the cluster resource (π^2) provided by the HPC center, Shanghai Jiao Tong University.

*zhjin@imr.ac.cn
†xyli@imr.ac.cn
‡lu@imr.ac.cn

[1] X. Y. Li, Z. H. Jin, X. Zhou, and K. Lu, Constrained minimal–interface structures in polycrystalline copper with extremely fine grains, Science **370**, 831 (2020).
[2] P. J. F. Gandy, D. Cvijović, A. L. Mackay, and J. Klinowski, Exact computation of the triply periodic D—('diamond') minimal surface, Chem. Phys. Lett. **314**, 543 (1999).
[3] See Supplemental Material at http://link.aps.org/supplemental/10.1103/PhysRevLett.127.136101 for methods and additional MD results, which includes Refs. [4–19].
[4] URL: https://science.sciencemag.org/content/suppl/2020/11/11/370.6518.831.DC1.
[5] D. H. Warrington and P. Bufalini, The coincidence site lattice and grain boundaries, Scr. Metall. **5**, 771 (1971).
[6] H. Grimmer, W. Bollmann, and D. H. Warrington, Coincidence–site lattices and complete pattern–shift in cubic crystals, Acta Cryst. **A30**, 197 (1974).
[7] R. W. Balluffi and A. P. Sutton, *Interfaces in Crystalline Materials* (Oxford, New York, 2007).
[8] S. Plimpton, Fast parallel algorithms for short-range molecular dynamics, J. Comput. Phys. **117**, 1 (1995).
[9] V. Borovikov, M. I. Mendelev, A. H. King, and R. LeSar, Effect of stacking fault energy on mechanism of plastic deformation in nanotwinned FCC metals, Model. Simul. Mater. Sci. Eng. **23**, 055003 (2015).
[10] C. A. Becker, F. Tavazza, Z. T. Trautt, and R. A. Buarque de Macedoc, Considerations for choosing and using force fields and interatomic potentials in materials science and engineering, Curr. Opin. Solid State Mater. Sci. **17**, 277 (2013).
[11] L. M. Hale, Z. T. Trautt, and C. A. Becker, Evaluating variability with atomistic simulations: The effect of potential and calculation methodology on the modeling of lattice and elastic constants, Model. Simul. Mater. Sci. Eng. **26**, 055003 (2018).
[12] URL: https://www.ctcms.nist.gov/potentials.
[13] A. Hashibon, A. Y. Lozovoi, Y. Mishin, C. Elsässer, and P. Gumbsch, Interatomic potential for the Cu–Ta system and its application to surface wetting and dewetting, Phys. Rev. B **77**, 094131 (2008).
[14] B.-J. Lee and J.-H. Shim, A modified embedded atom method interatomic potential for the Cu–Ni system, CALPHAD: Comput. Coupling Phase Diagrams Thermochem. **28**, 125 (2004).
[15] A. Stukowski, Visualization and analysis of atomistic simulation data with OVITO–the open visualization tool, Model. Simul. Mater. Sci. Eng. **18**, 015012 (2010).
[16] A. Stukowski, V. V. Bulatov, and A. Arsenlis, Automated identification and indexing of dislocations in crystal interfaces, Model. Simul. Mater. Sci. Eng. **20**, 085007 (2012).
[17] C. Kittel, *Introduction to Solid State Physics* (Wiley, New York, 2005).
[18] P. M. Anderson, J. P. Hirth, and J. Lothe, *Theory of Dislocations*, 3rd ed. (Cambridge University Press, Cambridge, England, 2017).
[19] Z. H. Jin, P. Gumbsch, K. Lu, and E. Ma, Melting Mechanisms at the Limit of Superheating, Phys. Rev. Lett. **87**, 055703 (2001).
[20] W. Xu, B. Zhang, X. Y. Li, and K. Lu, Suppressing atomic diffusion with the Schwarz crystal structure in supersaturated Al-Mg alloys, Science **373**, 683 (2021).
[21] To be published.
[22] H. A. Schwarz, Ueber die Minimalfläche, deren Begrenzung als ein von vier Kanten eines regulären Tetraeders gebildetes räumliches Vierseit gegeben ist, *Monatsberichte der Königlichen Akademie der Wissenschaften zu Berlin*, 149 (1865); H. A. Schwarz, *Gesammelte Mathematische Abhandlungen* (Springer, Berlin, Heidelberg, 1890).
[23] B. Riemann, Über die Fläche vom kleinsten Inhalt bei gegebener Begrenzung, Abhandlungen der Königlichen Gesellschaft der Wissenschaften zu Göttingen **13**, 3 (1867); B. Riemann, *Bernhard Riemann Collected Papers* (Kendrick Press, Heber City, 2004), pp. 287–337.
[24] A. H. Schoen, Infinite periodic minimal surfaces without self-intersections, NASA Technical Note TN D–5541, 1970.
[25] J. C. C. Nitsche, *Lectures on Minimal Surfaces I* (Cambridge University Press, Cambridge, England, 1989).
[26] P. J. F. Gandy and J. Klinowski, Exact computation of the triply periodic Schwarz P minimal surface, Chem. Phys. Lett. **322**, 579 (2000).
[27] W. Longley and T. J. McIntosh, A bicontinuous tetrahedral structure in a liquid–crystalline lipid, Nature (London) **303**, 612 (1983).
[28] Alan L. Mackay, Periodic minimal surfaces, Physica (B+C) (Amsterdam) **131**, 300 (1985).
[29] E. L. Thomas, D. M. Anderson, C. S. Henkee, and D. Hoffman, Periodic area–minimizing surfaces in block copolymers, Nature (London) **334**, 598 (1988).
[30] D. Hoffman, A new turn for Archimedes, Nature (London) **384**, 28 (1996).
[31] L. Kelvin (Sir William Thomson), On the division of space with minimum partitional area, Philos. Mag. **24**, 503 (1887).
[32] X. Zhou, X. Y. Li, and K. Lu, Enhanced thermal stability of nanograined metals below a critical grain size, Science **360**, 526 (2018).
[33] X. Zhou, X. Y. Li, and K. Lu, Size Dependence of Grain Boundary Migration in Metals under Mechanical Loading, Phys. Rev. Lett. **122**, 126101 (2019).
[34] C. A. Lambert, L. H. Radzilowski, and E. L. Thomas, Triply periodic level surfaces as models for cubic tricontinuous block copolymer morphologies, Phil. Trans. R. Soc. A **354**, 2009 (1996).
[35] V. Y. Gertsman and B. W. Reed, On the three–dimensional twin–limited Microstructure, Z. Metallkd. **96**, 1106 (2005).
[36] K. Miyazawa, Y. Iwasaki, K. Ito, and Y. Ishida, Combination rule of Σ values at triple junctions in cubic polycrystals, Acta Cryst. **A52**, 787 (1996).
[37] V. Randle, Y. Hu, and M. Coleman, Grain boundary reorientation in copper, J. Mater. Sci. **43**, 3782 (2008).

[38] G. Gottstein and L. S. Shvindlerman, *Grain Boundary Migration in Metals: Thermodynamics, Kinetics, Applications*, 2nd ed. (CRC Press, Boca Raton, 2010).

[39] J. W. Cahn and J. E. Taylor, A unified approach to motion of grain boundaries, relative tangential translation along grain boundaries and grain rotation, Acta Mater. **52**, 4887 (2004).

[40] R. W. Cahn, Topology of crystal grains, Nature (London) **250**, 702 (1974).

[41] F. N. Rhines, K. R. Craig, and R. T. Dehoff, Mechanism of steady-state grain growth in aluminum, Metall. Trans. **5**, 413 (1974).

[42] H. Gleiter, Nanostructured materials: Basic concepts and microstructure, Acta Mater. **48**, 1 (2000).

[43] K. Lu, Stabilizing nanostructures in metals using grain, and twin boundary architectures. Nat. Rev. Mater. **1**, 16019 (2016).